COMPDYN 2017
6th ECCOMAS Thematic Conference on
Computational Methods in Structural Dynamics and Earthquake Engineering
M. Papadrakakis, M. Fragiadakis (eds.)
Rhodes Island, Greece, 15–17 June 2017

EXPERIMENTAL VALIDATION OF IN-PLANE FRICTIONAL RESISTANCES IN DRY BLOCK MASONRY WALLS

Claudia Casapulla[1], **Luca U. Argiento**[1], **Carla Ceraldi**[1]

[1] University of Napoli "Federico II"
Department of Structures for Engineering and Architecture, Napoli, Italy
{casacla,lucaumberto.argiento,ceraldi}@unina.it

Keywords: Experimental Frictional Behavior, In-plane Loading, Masonry Shear Walls, Rocking-Sliding Failure Modes.

Abstract. *This paper presents the experimental and analytical validation of the lateral strength of dry block masonry walls under in-plane loading. The analytical evaluation of the in-plane frictional resistances activated at the onset of the rocking-sliding mechanisms is re-visited in order to account for the different contributions of the self weight of the wall and additional loads. It is assumed that the wall is arranged in a running bond pattern, with rigid blocks and dry contact interfaces governed by cohesionless Coulomb failure criterion. The accuracy and robustness of the analytical results are assessed by experimentally testing both the resultant frictional resistances and their applications points. Both pure sliding and rocking-sliding failure modes are simulated with a testing device designed and realized ad hoc (no standard equipments and procedures were found in the literature). A good agreement between the analytical and experimental results is shown for the selected cases.*

1 INTRODUCTION

In the past forty years, several approaches for modeling masonry structures have been developed to evaluate the seismic vulnerability of historic masonry buildings. Among these, many studies are based on the direct observation of recurrent damage and collapse mechanisms in seismic scenarios and are aimed at calculating the ultimate load factors by means of limit-state analysis [1].

In particular, the macro-block modelling approach has demonstrated to be useful for masonry buildings without a box-type behaviour, where frictional resistances might play a predominant role at the onset of in-plane and out-of-plane failure mechanisms [2-14]. According to it, each block represents a portion of masonry which remains undamaged and is separated from others by a number of localized cracking where the frictional resistances can take place. This modelling strategy relies on the advantage that the collapse load factor is easily computable by means of few equilibrium equations based on limit analysis methods. It could also be useful to further develop recent innovative research in the field of rocking rigid block dynamics [15-18].

Crucial to this approach is the assessment of the frictional resistances along the cracks.

In this paper, considering the masonry block wall as a single leaf wall arranged in a running bond pattern, the analytical model proposed in [19] for the calculation of in-plane frictional resistances was reconsidered to define more accurately the lateral strength of the wall. To this aim, a revisited formulation for the frictional resistances was presented by identifying two distinguished contributions, one due to the self weight of the wall and the other due to the possible overloading. Then the experimental validation of these analytical results was provided by investigating the effects of applying the horizontal loadings at different points along the vertical side face of the wall. The testing device was designed and realized ad hoc since no standard equipments and procedures were found in the literature and, to date, it does not appear that the frictional resistances of a dry stone masonry panel were ever tested. More details can be found in another work [20].

2 IN-PLANE FRICTIONAL RESISTANCES ALONG A CRACK

A rigid-perfectly plastic model with dry contact interfaces governed by cohesionless Coulomb failure criterion is herein adopted for the assessment of frictional resistances within in-plane loaded masonry walls, assumed to be single leaf walls arranged in a running bond pattern (Fig. 1). According to this model, the crushing of rigid blocks is ignored, the plastic dissipation is reduced to contact interfaces, in particular to bed joints, and the possible failure modes (rocking and/or sliding) take place along defined patterns of lines (cracks), which follow disposition of joints. Experimental and analytical investigation on 3D frictional behavior was recently carried out by Casapulla and Portioli [21, 22] to evaluate the frictional strength parameters in terms of shear, torsion and bending moments and combinations of them.

Although the limiting shear force due to friction at a single bed joint can easily be computed as the weight of the upper column of half-blocks multiplied by the friction coefficient (Coulomb's law), its resultant on all the bed joints along a given crack, also considering the presence of overloading, does not correspond in a simplistic way to the total weight of the moving portion times the friction coefficient. In fact, this resultant can only be derived according to two different formulations which actually give the same results [19]. One of these formulations is revisited in this paper in order to define more accurately the contributions of the self weight of the wall and the possible overloading.

The shape factor of the single unit depicted in Fig. 1(a) is defined as the angle $\alpha_b = \tan^{-1}(v/h)$, where $v = l/2$ and h and l are the height and the length of the unit, respectively. Also,

the shape factor of the wall in Fig. 1(b) of width L and height H is defined as the angle $\alpha_p = \tan^{-1}(L/H)$. The following considerations are limited to angles of crack $\alpha_c \leq \alpha_b$, as mechanisms with a greater angle of cracks are unlikely to occur under the current assumptions.

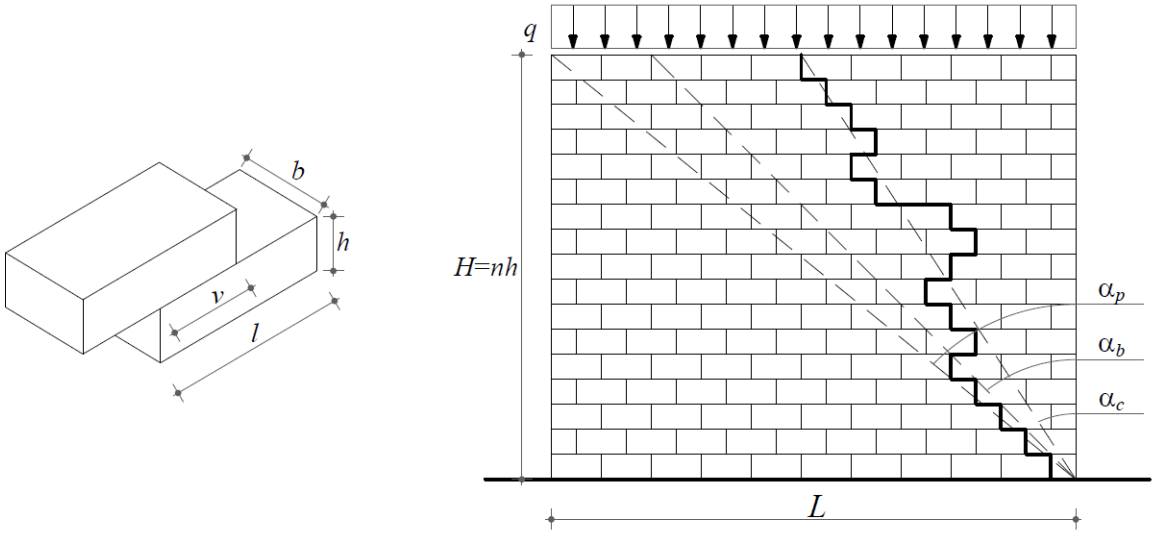

Figure 1: (a) Masonry unit dimensions; (b) inclinations for the unit and wall shape ratios and for the variable angle of crack.

2.1 Proposed formulation

The resultant frictional resistance on all the bed joints along a given crack only depends on the number of courses that the crack line actually crosses [5, 7].

In the following, this assumption is revisited only with reference to the case of $\alpha_c \leq \alpha_p$. In this case, typical for long walls, the total shear strength is independent of the angle of crack, as the number of rows crossed by the crack line is always that corresponding to the total height of the wall. It is also independent of whether the unit shape factor is greater or smaller than the wall shape factor. These results are described within the following two different conditions.

Case (a) $\alpha_b \leq \alpha_p$ (Fig. 2)

The total force F results from the sum of two contributions: F_W, related to the weight of the wall acting on all the bed joints and F_Q, related to the uniformly distributed load q for unit of length, acting at the top wall. It is worth noting that the distribution of these contributions along the height of the wall is linear for the former and uniform for the latter.

In particular, being n the number of rows crossed by the generic crack line, the limiting shear force due to friction at contact interface i, in absence of overloading, is given by the weight of the upper column of half-blocks multiplied by the friction coefficient f, i.e. according to the cohesionless Coulomb's law:

$$S_i = i\, f\, W_b \qquad \text{i} = 1, 2, 3, \ldots, \text{n} \tag{1}$$

where $W_b = \gamma bvh$ is the weight of a single half-block (γ is the specific weight of the material). The first resultant will be:

$$F_W = \sum_1^n S_i = \gamma bhv \frac{n(n+1)}{2} f \tag{2}$$

and it will be applied at 2/3 of the height of the cracked part from the top of the panel, since S_i linearly increases from the top to the bottom wall [13, 19].

On the other hand, the resultant due to the overload is expressed in the form:

$$F_Q = qnvf \tag{3}$$

and it is applied at half-height of the wall, as illustrated in Fig. 2.

The total frictional resistance is therefore the sum of Eqs. (2) and (3), i.e.:

$$F = F_W + F_Q \tag{4}$$

which is clearly independent of the angle of crack. Its application point can easily be obtained with the expression:

$$y_F = \frac{F_W nh/3 + F_Q nh/2}{F_W + F_Q} \tag{5}$$

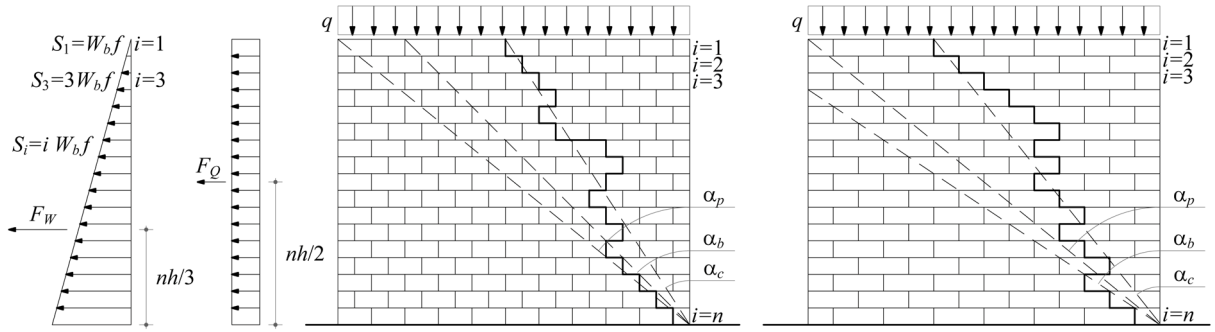

Figure 2: Proposed frictional resistances for: Case (a) with $\alpha_b \leq \alpha_p$ and Case (b) with $\alpha_b \geq \alpha_p$.

Case (b) $\alpha_b \geq \alpha_p$ (Fig. 2)

As introduced above, also in this case the number of surfaces crossed by the crack line does not change with α_c and it is always equal to the total number of courses in the panel considered. This allows obtaining the same total shear strength as Case (a), i.e. equal to Eq. (4).

3 EXPERIMENTAL VALIDATION OF FRICTIONAL RESISTANCES

A series of laboratory tests were carried out to experimentally validate the frictional resistances described in the previous section. To this aim it was verified that a horizontal point-load applied, with opposite sign, to the same application point of the resultant frictional resistance exerted by the wall effectively implied pure sliding failure mode, while involving a mixed rocking-sliding failure when different application points were considered.

The tested wall was 800 mm x 468 mm x 50 mm (length x height x width) in size and had twelve courses of stretcher blocks. It was constructed using 100 mm x 39 mm x 50 mm (length x height x width) Neapolitan tuff stones arranged in a running bond pattern and with an average unit weight equal to 13.1 kN/m^3. All masonry blocks were cut mechanically leaving a smooth surface and placed within the wall without mortar (dry joints). The friction coefficient between the faces of the tuff stones was calculated experimentally using the same setup of the wall and was found to be equal to 0.52. In order to allow the same frictional resistance at each involved contact surface, an additional course of stretcher tuff stones horizontally constrained was placed between the tested wall and the rigid and fixed supporting base.

Different loading conditions were considered to simulate both pure sliding and mixed rocking-sliding failure modes.

3.1 Test setup

The test setup was designed and realized ad hoc since no standard equipments and procedures were found in the literature. This consisted of the application of a horizontal point-load to the side face of the dry stone masonry wall specimen by means of a universal electromechanical testing machine, as schematically shown in Fig. 3.

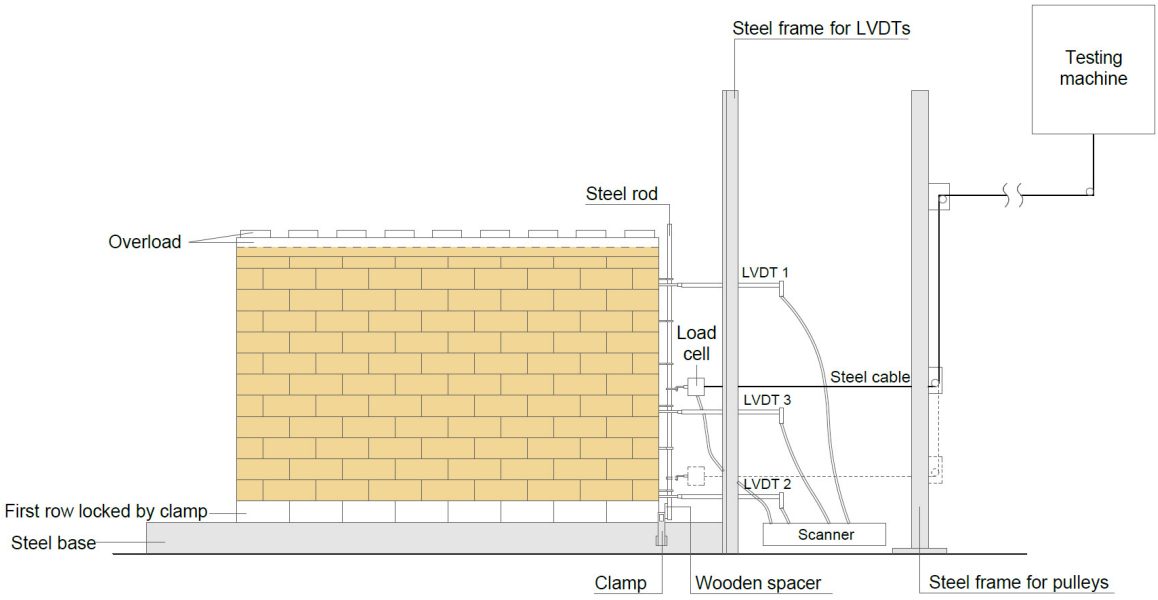

Figure 3. Test setup.

In order to simulate the predicted failure modes and to distribute the point-load along the vertical side face of the wall, the horizontal load was applied to a vertical steel rod (550 mm long, 10 mm diameter) inserted in six eye screws attached to the half-block on alternating stretching courses. The rod was rigid enough to support the maximum load used during the tests without deformation. It was also suspended on the upper eye screw to avoid any contact with the base support and was unilaterally constrained at its base in horizontal direction through a wooden spacer to prevent inward displacement during its rotation. In fact, it is worth underlying that to avoid interpenetration of blocks this rod was only allowed to translate outward and unilaterally rotate about the pivot point.

The loading scheme was designed to apply the point-load at a variable height within the vertical midplane of the wall and to involve all the possible in-plane displacements transmitted by the steel rod. To activate the failure mechanisms, a monotonically increasing horizontal force was applied using the testing machine. A steel cable, supported by a system of small pulleys and a steel frame, was used to connect the steel rod to the actuator of the testing machine running in the vertical direction. In order to apply the point-load along the horizontal direction, the lower pulley was allowed to shift vertically. The load was applied under displacement control at a constant rate of 5 mm/min, using the control system of the testing machine to calibrate the speed of the vertical actuator.

The force was measured using a load cell with a maximum capacity of 500 N and an acquisition frequency of 10 Hz. The displacements were measured using three Linear Variable Displacement Transducers (LVDT) with a displacement range of ± 50 mm. These LVDTs,

supported by the steel frame, were positioned to the first, fourth and last half-block of the side face of the tested wall from its top to the bottom. The purpose of the LVDTs was to measure the displacements along the height of the wall to distinguish the pure sliding mechanisms from the rocking-sliding ones. The load cell and the transducers were connected to a digital scanner to acquire forces and displacements.

In some tests the wall was subjected to a constant overload of 320 N, which was about 34% larger than its self weight. This overload was uniformly distributed along the top wall through the use of a steel H-beam, weighing 66 N and placed with horizontal web (Fig. 6(c)), supporting nine cast iron cylinders, each with an average weight of about 28.2 N (254 N total cylinders).

3.2 Testing programme

The experimental programme was planned in order to validate the frictional resistance of the tested dry stone masonry wall in the cases of absence (Test 1) or presence (Test 2) of the overload. These cases were expected to involve pure sliding failure modes only. The additional Tests 3 and 4, implying mixed rocking-sliding mechanisms, allowed to validate the application point of the frictional resistance both in the absence and presence of overload.

Experimental tests were carried out for Case (a) only ($\alpha_c \leq \alpha_b \leq \alpha_p$), since Case (b) ($\alpha_c \leq \alpha_p \leq \alpha_b$) can be directly derived from Case (a). Table 1 summarizes the chosen values of the overload and the application points of the point-load for each test. The last row is referred to the values of the application points measured from the bottom of the rod instead of the bottom of the wall to take into account the pivot point in the cases of rotation of the rod. The distance between the pivot point and the bottom of the wall was measured to be $d = (z - y) \approx 20$ mm.

Table 1. Experimental tests with the chosen values of the overload and the application points of the force.

	Pure sliding failure		*Rocking-sliding failure*	
	Test 1	*Test 2*	*Test 3*	*Test 4*
Overload, Q [N]	-	320	-	320
Application point from the bottom of the wall, y [mm]	156	212	312	312
Application point from the bottom of the rod, z [mm]	176	232	332	332

The application points of the force for Tests 1 and 2 were determined using Eq. (5), which considers the effects of both the self weight and the overload. Instead, the force was applied at 2/3 of the wall height for Tests 3 and 4.

3.3 Experimental results and comparisons

3.3.1 Pure sliding failure

Wall panel Test 1 was carried out without overloading and by applying the horizontal force at 1/3 of the wall height from its bottom (156 mm).

The results of the test were reported both in terms of failure mode and of the average frictional resistance to be compared with analytical results.

The first evidence observed in Fig. 4(a) is that effectively pure sliding mechanism occurred when considering the chosen application point. In fact, although a slightly smeared distribution of sliding movements can be detected along the courses, a clear separation of a portion of

wall with nearly the same amount of the total horizontal displacement for each course can be distinguished.

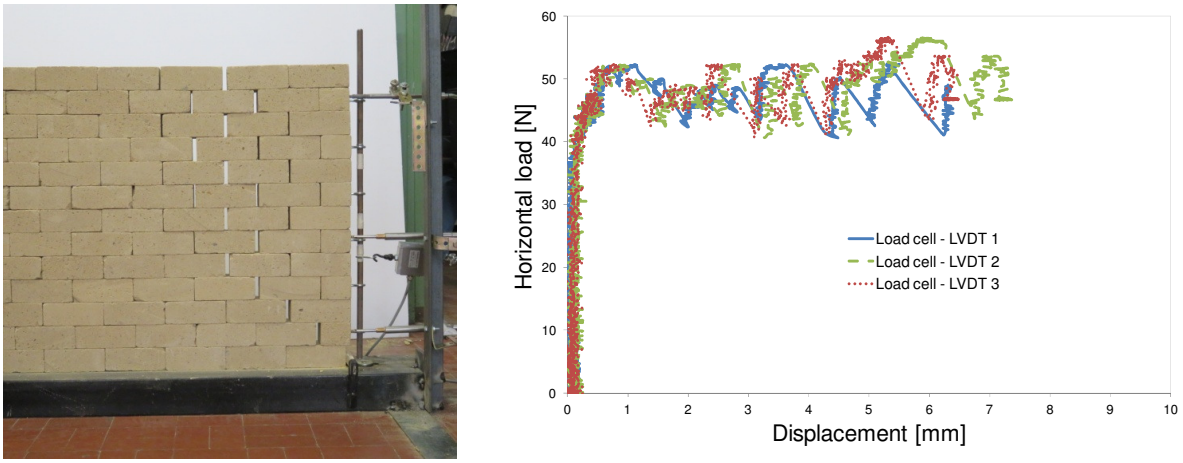

(a) (b)

Figure 4: (a) Failure mode for the wall specimen and (b) load-displacement curves for Test 1.

In Fig. 4(b) the results of Test 1 are plotted in terms of three load-displacement curves derived from the combinations of the load cell with the three positioned LVDTs. For all the graphs reported in this section, the upper displacement transducer was LVDT 1 (blue continuous line), while LVDT 2 (green dashed line) and LVDT 3 (red dotted line) were the intermediate and the lower ones, respectively. As expected, the signals registered by the three LVDTs were nearly coincident, with an almost vertical branch representing the rigid behavior of the block interfaces and the maximum load occurring at the first noticeable movement. Although it appears quite difficult to identify the first noticeable movement and the corresponding load, it can be reasonable to assume the maximum load in the range 0-1 mm, i.e. $F = 51.2$ N in this case. The displacements registered after this point show the stick-slip behaviour which is typical of frictional sliding [23]. However, although the kinematics of the failure is beyond the scope of this paper, it is worth noting that the enhancement of displacement occurred without substantially increase in the loading force.

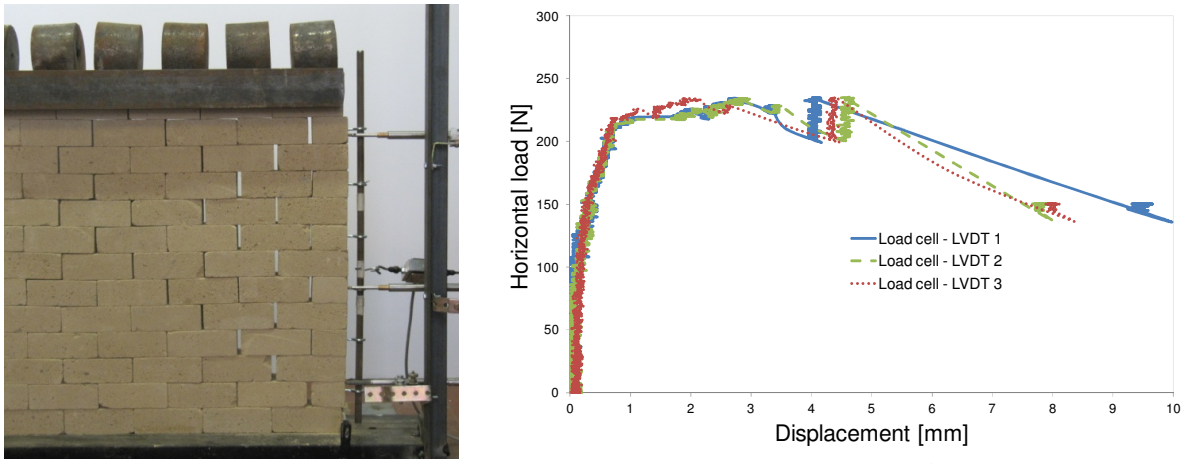

(a) (b)

Figure 5: (a) Failure mode for the wall specimen and (b) load-displacement curves for Test 2.

The second test (Test 2), considering the overload applied on the top wall, was carried out by applying the horizontal force at the distance from the bottom of the wall obtained using Eq. (5), i.e. 212 mm. Also in this case an actual pure sliding failure can be observed (Fig. 5(a)), though the moving portion of the wall had a different shape and could be identified as a triangular block. The results in terms of load-displacement curves are reported in Fig. 5(b) where trends similar to the curves in Fig. 4(b) can be observed. The first almost vertical branch can still represent the rigid behaviour of the block interfaces (the displacements less than 1 mm can be disregarded), while the stick-slip behavior after the onset of the mechanism appeared less pronounced. The maximum load was reasonably chosen as F = 207.1 N.

These first results were a clear indication of the correctness of the chosen application points obtained according to Eq. (5) and may effectively allow validating the linear and constant distributions of the frictional resistances described in the previous section. However, a further confirmation of the good agreement with analytical results will be shown later on within the comparisons between the experimental and predicted values of the applied horizontal force.

3.3.2 Rocking-sliding failure

Tests 3 and 4 were carried out to demonstrate that mixed rocking-sliding mechanisms may occur when the application points are chosen different from those activating pure sliding failure modes, in the absence and presence of overload, respectively (Fig. 6).

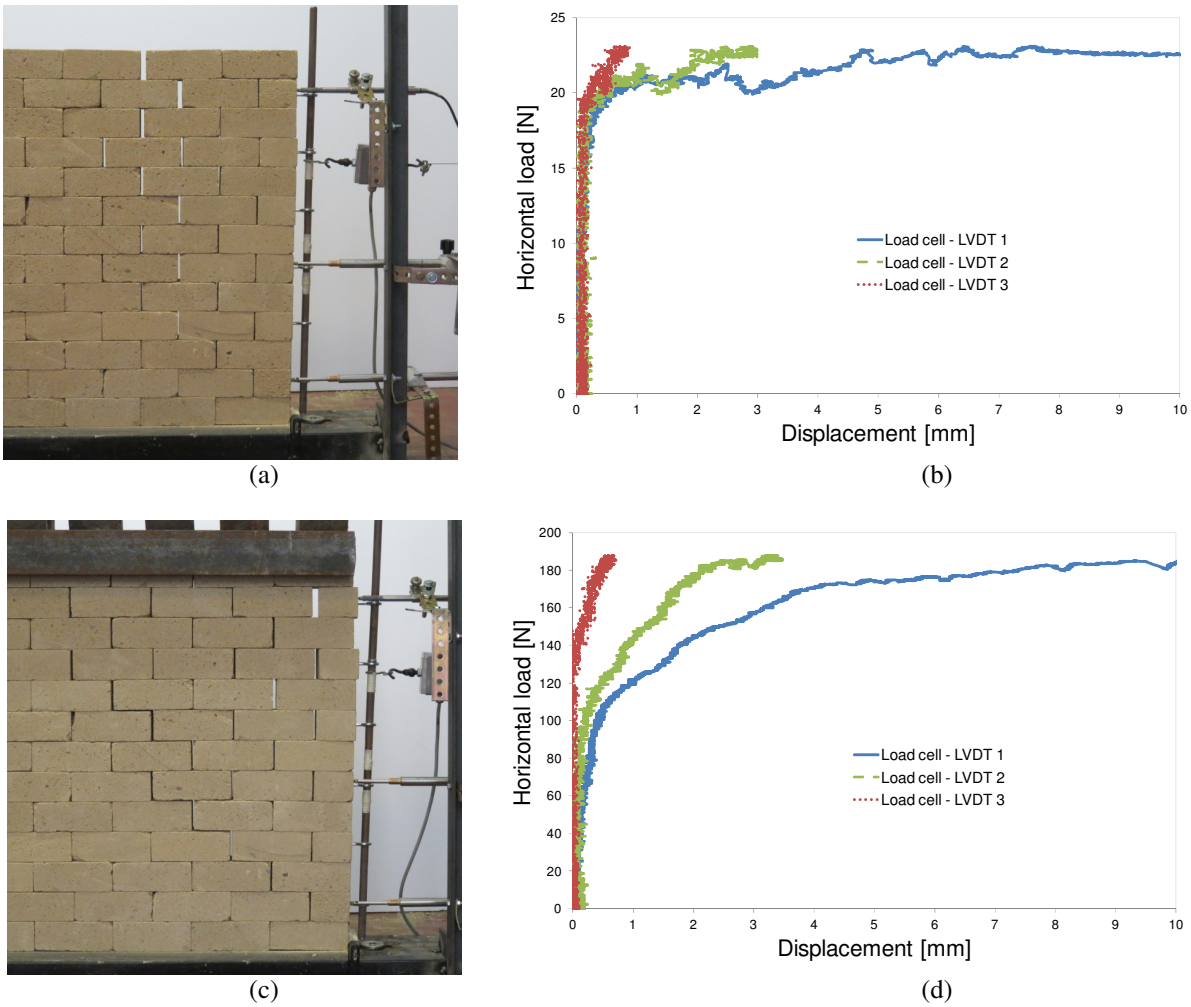

Fig. 6. Failure mode for the wall specimen and load-displacement curves for (a-b) Test 3, (c-d) Test 4.

In these figures, the failure modes and the corresponding load-displacement curves are reported for such tests, where the activated rocking-sliding mechanisms can be observed for all cases. In particular, Fig. 6(a) shows that the portion of the wall moving outward for Test 3 is quite similar to that in case of pure sliding (Fig. 4(a)), but with horizontal displacements increasing from the bottom to the top, due to the rotation of the steel rod about the pivot point. A similar phenomenon can be observed in presence of overloading for Test 4 in Fig. 6(c), where the rotation of the rod appeared amplified because of the greater displacements of the upper blocks. The load-displacement curves reflected the observed failure modes through the registration of quite linear distributions of the displacements, increasing from the lower LVDT 3 to the upper LVDT 1, when reached the applied loads activating the mechanisms. Considering the first noticeable movement of the upper LVDT 1 in the range 0-1 mm (as also assumed for pure sliding failure), these maximum loads were reasonably chosen as F = 21.1 N and F = 119.3 N for Tests 3 and 4, respectively.

3.3.3 Comparisons with analytical results

In Table 2 all the experimental results described above were compared to those obtained by the analytical formulations presented in Section 2, in terms of applied horizontal force. Both failure modes of pure sliding and rocking-sliding were considered.

In the cases of pure sliding mechanisms, i.e. Tests 1 and 2, the values of the frictional resistances and the applied horizontal loads were directly compared each other and Eq. (4) was used for analytical results, since no level arms must be computed. In the cases of rocking-sliding failure (Tests 3 and 4), instead, it is worth underlining that the analytical values of the applied horizontal loads were obtained through the rotational equilibrium of the steel rod about the pivot point. This means that the predicted forces, reported in Table 2, were obtained by the following relation:

$$F_1 = \frac{F\left(y_F + d\right)}{z} \tag{6}$$

where F and y_F are given by Eqs. (4) and (5), respectively, z is the distance of the application point from the bottom of the rod (Table 1) and d is the difference of about 20 mm between the bottom of the rod and the bottom of the wall, as introduced above in this section.

The comparison of the analytical results against experimental evidence shows that the predicted limiting forces agree well with the observed experimental results, both in terms of the frictional resistance and of its application point.

Table 2. Comparison of experimental and analytical results.

Pure sliding failure					
	y [mm]	z [mm]	Exp F [N]	Analytical F [N], Eq. (4)	Diff. Analytical vs. exp. [%]
Test 1	156	176	51.2	50.6	-1.2
Test 2	212	232	207.1	175.4	-15.3
Rocking-sliding failure					
	y [mm]	z [mm]	Exp F [N]	Analytical F_1 [N], Eq. (6)	Diff. Analytical vs. exp. [%]
Test 3	312	332	21.1	23.8	12.8
Test 4	312	332	119.3	118.9	-0.3

In particular, the frictional resistances assessed by the formulations proposed in Section 2 were validated by the experimental results for Tests 1 and 2, which show a relatively small percentage difference of about 1% and 15%, respectively. Moreover, it should be noted that

the analytical results are conservative with respect to the experimental ones and that the failure mode was assessed as pure sliding for both test performances.

A good agreement between the results can also be observed for Tests 3 and 4, which confirmed the correctness of the application points of the predicted frictional resistances in the cases when rocking-sliding failure modes were involved.

The percentage difference between the analytical - still conservative - and measured forces for Test 4 was effectively very small, i.e. about 0.3%, confirming the robustness of the analytical formulations, while an unconservative result was registered for Test 3, with about 13% of percentage difference (positive sign). This can be explained by the general observation that the experimental tests are locally influenced by some random factors, e.g. variations of normal pressure force or inhomogeneous asperity of contacting surfaces, which could vary from test to test. Notwithstanding, the percentage difference registered for Test 3 still was relatively small and the failure mode observed in Fig. 6(a) still confirmed the validity of the proposed formulations.

4 CONCLUSIONS

In this paper the lateral strength of dry block masonry walls under in-plane loading was measured by frictional resistances. Assuming the wall arranged in a running bond pattern, with rigid blocks and dry contact interfaces governed by cohesionless Coulomb failure criterion, its lateral strength was assessed by accounting for two contributions, one due to the self weight of the wall and the other due to the overloading. This allowed obtaining more accurate results for the resultant frictional resistances, as confirmed by the experimental investigation carried out to validate the analytical formulations. Both pure sliding and rocking-sliding failure modes were simulated with the testing device designed and realized ad hoc (no standard equipments and procedures were found in the literature).

ACKNOWLEDGMENTS

The authors acknowledge the sponsorship of the Italian Civil Protection, through the RELUIS Project - Line: Masonry Structures (2017). The authors wish to express their gratitude to Mr. Mario Torricella from the Departmental Test Laboratory in Naples, for the development of the test setup, and Mr. Domenico Imperatrice from the same Laboratory, for his assistance in the execution of the tests.

REFERENCES

[1] P. Roca, M. Cervera, G. Gariup, L. Pelà, Structural Analysis of Masonry Historical Constructions. Classical and Advanced Approaches. *Archives of Computational Methods in Engineering*, **17**, 299-325, 2010.

[2] D.C. Drucker, Coulomb friction, plasticity and limit loads. *Journal of Applied Mechanics*, **21**(1), 71-74, 1954.

[3] R.K. Livesley, Limit analysis of structures formed from rigid blocks. *International Journal of Numerical Methods in Engineering*, **12**, 1853-1871, 1978.

[4] T.E. Boothby, Stability of masonry piers and arches including sliding. *Journal of Engineering Mechanics*, **120**, 304-319, 1994.

[5] C. Casapulla, Dry rigid block masonry: safe solutions in presence of Coulomb friction. *Advances in Architecture Series*, **7**, 251-261, 2001.

[6] A. Orduña, *Seismic assessment of ancient masonry structures by rigid blocks limit analysis*. PhD Thesis, University of Minho, Guimarães, Portugal, 2003.

[7] C. Casapulla, D. D'Ayala, In-plane collapse behaviour of masonry walls with frictional resistances and openings. P.B. Lourenço, P. Roca, C. Modena, S. Agrawal eds. *5th International Conference on Structural Analysis of Historical Constructions (SAHC06)*, New Delhi, India, vol. 2, November 6-8, 2006.

[8] T. Tran-Cao, *Collapse analysis of block structures in frictional contact*. PhD thesis, The University of New South Wales, Sydney, Australia, 2009.

[9] C. Casapulla, A. Maione, Out-of-plane local mechanisms in masonry buildings. The role of the orientation of horizontal floor diaphragms. J. Ingham, M. Dhanasekar, M. Masia eds. *9th Australasian Masonry Conference*, Queenstown, New Zealand, February 15-18, 2011.

[10] G. Milani, M. Pizzolato, A. Tralli, Simple numerical model with second order effect for the out-of-plane loaded masonry walls. *Engineering Structures*, **48**, 98-120, 2013.

[11] P.B. Lourenço, Masonry modeling. M. Beer, I.A. Kougioumtzoglou, E. Patelli, S.-K. Au eds. *Encyclopedia of Earthquake Engineering*, Reference work, 1-13, 2014.

[12] C, Casapulla, A. Maione, Formulating the torsion strength of dry-stacked stone blocks by comparing convex and concave contact formulations and experimental results. *Indian Journal of Science and Technology*, 9(46), 107346, 2016.

[13] C. Casapulla, L.U. Argiento, The comparative role of friction in local out-of-plane mechanisms of masonry buildings. Pushover analysis and experimental investigation. *Engineering Structures*, **126**, 158-173, 2016.

[14] C. Casapulla, L.U. Argiento, Non-linear kinematic analysis of masonry walls out-of-plane loaded. The comparative role of friction between interlocked walls. *6th International Conference on Computational Methods in Structural Dynamics and Earthquake Engineering*, Rhodes Island, Greece, June 15-17, 2017.

[15] C. Casapulla, A. Maione, Free damped vibrations of rocking rigid blocks as uniformly accelerated motions. *International Journal of Structural Stability and Dynamics*, DOI: http://dx.doi.org/10.1142/S0219455417500584, 2016.

[16] C. Casapulla, A. Maione, Critical response of free-standing rocking blocks to the intense phase of an earthquake. *International Review of Civil Engineering*, **8**(1), 1-10, 2017.

[17] L. Giresini, Energy-based method for identifying vulnerable macro-elements in historic masonry churches. *Bulletin of Earthquake Engineering*, **44**(13), 919-942, 2015.

[18] L. Giresini, M. Sassu, Horizontally restrained rocking blocks: evaluation of the role of boundary conditions with static and dynamic approaches. *Bulletin of Earthquake Engineering*, **15**(1), 385-410, 2016.

[19] C. Casapulla, F. Portioli, A. Maione, R. Landolfo, A macro-block model for in-plane loaded masonry walls with non-associative Coulomb friction. *Meccanica*, **48**(9), 2107-2126, 2013.

[20] C. Casapulla, L.U. Argiento, In-plane frictional resistances in dry block masonry walls and rocking-sliding failure modes revisited and experimentally validated, *Composites Part B*, under review.

[21] C. Casapulla, F. Portioli, Experimental and analytical investigation on the frictional contact behavior of 3D masonry block assemblages. *Construction and Building Materials*, **78**, 126-143, 2015.

[22] C. Casapulla, F. Portioli, Experimental tests on the limit states of dry-jointed tuff blocks. *Materials and Structures*, **49**(3), 751-767, 2016.

[23] B. Feeny, A. Guran, N. Hinrichs, K. Popp, A historical review on dry friction and stick-slip phenomena. *Applied Mechanics Reviews*, **51**(5), 321-341, 1998.